Journal of
Nuclear Engineering

MDPI

Article

Heat Pipe-Based DEMO Divertor Target Concept: High Heat Flux Performance Evaluation

Wen Wen [1,*], Bradut-Eugen Ghidersa [1], Wolfgang Hering [1], Jörg Starflinger [2] and Robert Stieglitz [1]

[1] Institute for Neutron Physics and Reactor Technology, Karlsruhe Institute of Technology, 76344 Eggenstein-Leopoldshafen, Germany
[2] Institute of Nuclear Technology and Energy Systems, University of Stuttgart, 70569 Stuttgart, Germany
* Correspondence: wen.wen@kit.edu

Abstract: The use of heat pipes (HP) for the DEMO in-vessel plasma-facing components (PFCs) has been considered because of their high capacity to transport the heat from a heat source to a heat sink by means of the vaporization and condensation of the working fluid inside and their ability to enlarge the heat transfer area of the cooling circuit substantially. Recent engineering studies conducted in the framework of the EUROfusion work package Divertor (Wen et al, 2021) indicate that it is possible to design a heat pipe with a capillary limit above 6 kW using a composite capillary structure (wherein axial grooves cover the adiabatic zone and the condenser, and sintered porous material covers the evaporator). This power level would correspond to an applied heat flux of 20 MW/m^2, rendering such a design interesting with respect to a divertor target concept. To validate the results of the initial engineering analysis, several experiments have been conducted to evaluate the actual performance of the proposed heat pipe concept. The present contribution presents the experiment's results regarding the examination of the operating limits of two different designs for an evaporator: one featuring a plain porous structure, and one featuring ribs and channels.

Keywords: heat pipe; high heat flux experiment; plasma facing component; wick porous

Citation: Wen, W.; Ghidersa, B.-E.; Hering, W.; Starflinger, J.; Stieglitz, R. Heat Pipe-Based DEMO Divertor Target Concept: High Heat Flux Performance Evaluation. *J. Nucl. Eng.* **2023**, *4*, 278–296. https://doi.org/10.3390/jne4010021

Academic Editors: Stjepko Fazinić, Tonči Tadić and Ivančica Bogdanović Radović

Received: 31 October 2022
Revised: 21 February 2023
Accepted: 23 February 2023
Published: 9 March 2023

1. Introduction

DEMO in-vessel plasma-facing components (PFCs) are exposed to high heat fluxes. In particular, the divertor targets will have their plasma-facing side subjected to both particle bombardment and heating via radiation. These loadings produce surface heat fluxes with peak values of 10 MW/m^2 or more at the strike point. To find a solution that can withstand such loading conditions and has a suitable lifetime, the work package 'Divertor' from the EUROfusion was launched in 2014. The baseline solution features cooling pipes made of Cu–Cr–Zr and incorporates W-blocks as armor [1]. However, as the heat load of these components is asymmetric, with most of the heat being applied on their plasma-facing side, the heat transfer area is limited to a small portion of the pipe's circumference. Increasing this area would benefit the cooling system by reducing some of its requirements. One way of achieving this would be to insert heat pipes between the tungsten armor and the cooling circuit. Heat pipes are a capillary-driven, two-phase system that can transport heat by vaporizing and condensing a working fluid with high effective thermal conductivity. Taking advantage of their high conductivity, the surface heat from the DEMO Divertor target's plasma-facing side can efficiently be transported into the cooling fluid through the heat pipe condenser, which can also be designed with a large contact area. Thus, the local heat flux can be maintained well below the critical values.

The idea of using heat pipes in fusion applications and plasma-facing components is not new. In the literature, several studies have investigated various types of porous media heat exchangers, including heat pipes for applications. For instance, some studies [2,3] consider liquid metal as the working fluid, especially lithium, used to increase high-temperature heat pipes' heat flux capacity. The solutions proposed in these studies were

tested both in normal and magnetic field environments. However, the lithium-based heat pipes' working temperature (about 1100 °C) is very close to the tungsten recrystallization temperature, thus introducing additional constraints on the armor thickness.

Water-based heat pipes have already been considered in the past for fusion high-heat flux applications [4]. Four Monel/water U-shaped thermosyphon heat pipes with a nickel-plated copper porous felt metal wick shield were designed to handle local incident heat fluxes as high as 2 MW/m^2 and to operate between 373 and 573 K (100 and 300 °C).

Accordingly, a divertor target concept based on heat pipe technology was proposed in [5]. The target comprises many parallel cylindrical heat pipes with the armor attached to the evaporator end. The condenser end of the heat pipe is inserted in a cooling channel, forming a staggered rod pattern. The dimensional analysis presented in [5] indicates that a unit, as shown in Figure 1b, would have its applicable operating limits above 5.7 kW of the transported power. This value corresponds to a heat flux of 20 MW/m^2 on the armor's surface. The proposed design, called a Divertor Heat Pipe (DIV-HP), uses a combination of capillary structures with axial grooves (enclosed by a mesh screen) at the condenser and adiabatic zones and a sintered porous structure situated by the evaporator.

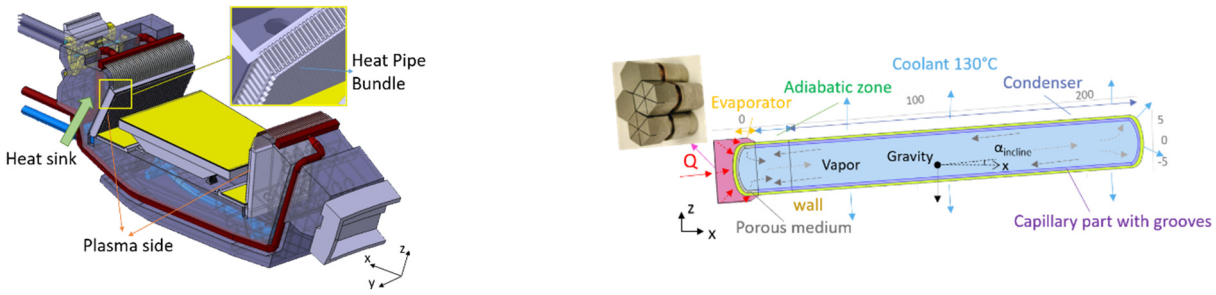

(**a**) (**b**)

Figure 1. EU-DEMO divertor concept featuring a heat-pipe-based target from [1]: (**a**) target concept and its integration with the divertor cassette; (**b**) DIV-HP heat pipe unit dimensioned with proposed tungsten armor.

The studies in [5] did not discuss the boiling limit of such a pipe because the design features channels and an open porosity evaporator, and such a limit should not be critical [6]. However, given the high peak heat fluxes occurring on the evaporator side, it would be more prudent to obtain a better sense of the operational limits of the heat pipe before proceeding with the manufacturing and testing of a full-scale DIV-HP heat pipe. As such, a dedicated experiment investigating this aspect was performed. The present contribution introduces the design of the test mock-up focusing on the evaporator and discusses the experimental setup in detail. Special attention is given to the instrumentation and specific aspects of power deposition evaluation through calorimetric methods. Then, the results of the first series of experiments with surface heat fluxes up to 1.3 MW/m^2 are discussed. To conclude, the progress and the plans for future studies are presented.

2. Mock-Up Design and Layout of the Experimental Setup

The heat pipe design proposed in [5] uses a sintered porous structure in the evaporator zone, thus ensuring a high capillary operating limit. This structure covers the heat pipe's complete (hot) end attached to the tungsten armor. The evaporator has a hemispherical part with a mean radius of 15 mm and extends 3 mm in the cylindrical part of the pipe. The thickness of the porous layer at the evaporator end is 1 mm with a porosity of around 50%. For the boiling limit, simple engineering formulas, as proposed in [6] for an HP with a cylindrical geometry, rely on several parameters that must be estimated for the porous structure. However, the results vary significantly depending on the assumptions used to calculate those parameters.

For this reason, it was decided to investigate the operating limits of the evaporator experimentally. The objective was to obtain a mock-up that retains most of the selected heat pipe's design characteristics while relaxing certain features to simplify manufacturing and keep the costs for the experimental setup within reasonable margins. Given that the new test mock-up is only designed for investigating the evaporator to distinguish between the DIV-HP and the present one, the current experimental design will hereafter be referred to as Heat Pipe for Evaluating an Evaporator (HPEE).

Thus, the mock-up will have an evaporator similar to the original heat pipe, and it should be capable of transferring at least 5.7 kW between the evaporator and the condenser. A porous structure was chosen to obtain a similar porosity and particle size as the one presented in [5] in the sense that the capillary driving force of the heat pipe should not be affected. In addition, the capillary grooves designed for water to reach the evaporator have the same shape as the DIV-HP with only a tiny difference. The channel depth is smaller for the HPEE (0.5 mm plus a rounded end with a radius of 0.15 mm as compared to 1 mm for the original design) to compensate for the fact that, for the HPEE, the number of channels is greater due to the larger circumference of the body. The material used for the heat pipe wall is CuCrZr, which is the same material selected for the DIV-HP in [5].

The design intended to have a mock-up unit whose performance is solely driven by the boiling limit/evaporator performance. As such, a vertical arrangement of the heat pipe was selected to increase the HPEE's capillary limit above that of the DIV-HP. The condenser is positioned above the evaporator, so gravity will act positively on the water from the condenser to the evaporator, thus adding to the capillary driving force.

2.1. Evaporator

Considering the high-pressure operating conditions inside the HPEE at high power loads as well as the wall thickness limitation with respect to heat conductivity, the heat load area should be reduced as close as possible to the size of the DIV-HP evaporator. This size corresponds to the sum of the hemispherical and cylindrical parts of the pipe (400 mm^2). Hence, for the HPEE, the evaporator is essentially a flat disk with a diameter of 25 mm. The heated surface (490 mm^2) is slightly larger than the wick structure surface of the DIV-HP due to the coolant flow's path length. Hence, this design decision is conservative. In addition, when the design was concluded, it was planned to use a laser machine to apply the surface load. The optics selected for the experiment can generate a 19 mm by 19 mm beam spot, while the 50% peak power concentrates on a 15 mm by 15 mm surface.

According to the stress calculations, the minimum thickness of the CuCrZr plate is 1.5 mm. Finally, the wall thickness is 2 mm with a safety margin, and a 2 mm tungsten plate was added, which covered the CuCrZr plate, as in shown Figure 2. The primary purpose of the tungsten armor is to protect the temperature sensors installed on the CuCrZr wall's surface. In addition, since it was decided that the heat load should be applied using a power laser machine, a tungsten cover would have better absorption properties with respect to the laser beam than a copper-based material.

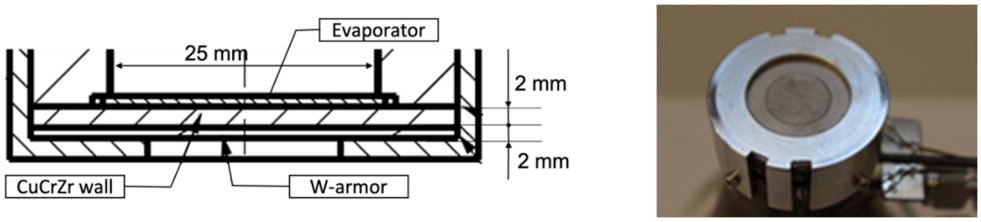

(**a**) (**b**)

Figure 2. Depiction of HPEE. (**a**) Depiction with dimensions of HPEE evaporator-end with W-plate; (**b**) top view of the evaporator surface with W-plate and protective cover.

2.2. Wick Structure

The initial intention was to have an HPEE wick structure identical to that of the DIV-HP, featuring the same grooves in the adiabatic zone and a copper-sintered porous plate at the evaporator side. However, all the evaporator samples manufactured using copper powder for the sintered structure suffered from adhesion problems and failed to be appropriately integrated into the final mock-up. As a consequence, bronze was selected as the porous material, specifically, type B200, which has high porosity of 0.47, a grain radius of 400 µm, and permeability of 1.54×10^{-10} m^2. This sintered structure showed excellent stability and had an apparent open porosity. However, by selecting this option, two main aspects impacted the experimental design:

- The thickness of the wick porous B200 on the CuCrZr plate was increased from 1 mm to 2 mm due to the larger grain size of the sintered material (B200);
- The maximum heat flux that the B200-mockup could receive was only 4 MW/m^2, which was mainly due to the sintered material's low heat conductivity (40 $W/m/K$), thus resulting in an increased wall temperature. The heat flux of 4 MW/m^2 corresponds to the loading at which the CuCrZr wall approaches its operational limits.

One possible reason that drying occurs in a porous structure is that the accumulation of bubbles blocks the liquid flow entering a particular evaporator area. Hence, high-performance evaporators with channels or rib structures are used in heat pipe applications to mitigate this issue [7]. Therefore, to investigate the impact of such features on the heat pipe's performance, it was decided to investigate two types of sintered structures in two mock-ups: mock-up-1, with one plain evaporator (see Figure 3a, and mock-up-2, with a porous structure featuring a pattern of channels on its surface Figure 3b.

(**a**) (**b**)

Figure 3. Porous structure on CuCrZr plate: (**a**) original shape; (**b**) version with channels.

Both choices of sintered porous structures mounted on the CuCrZr plate are shown in Figure 3. The various evaporator parameters are listed in Table 1, including the adiabatic zone's channel number and dimensions.

Table 1. Parameters of wick structures: grooves at adiabatic zone and sintered porous evaporators.

Parameters	Symbol	Value
Width of groove	w	0.3 mm
Depth of groove in the evaporator	h	0.65 mm
Number of grooves	N_g	125
Sintered porous configuration for mock-up-1		
Height of porous evaporator (Bronze)	h_e	2 mm
The grain size of the sinter's	r_p	~400 um
porosity	ε	0.47
Sintered porous configuration for mock-up-2		
Height of porous evaporator (Bronze)	h_e	2 mm
The grain size of the sinter's	r_p	~400 um
porosity	ε	0.47
Width of porous channels	w_{pc}	1 mm
Depth of porous channels	h_{pc}	1 mm
Number of porous channels and their length	N_{pc}	4 × 10 mm + 4 × 6 mm

2.3. Reservoir for Volume Change

When the heat flux changes from 1 MW/m^2 to 20 MW/m^2, the liquid volume required for the heat pipe's operation will change [8]. If the filling procedure is executed for the maximum loading, the excess liquid will gather on top of the evaporator, creating a pool of water for testing at a low power range. This would result in a pool-boiling-dominated process over the evaporator, which is characteristic of a thermosyphon, instead of our intended goal, i.e., boiling inside a porous structure. To avoid this, we created a small reservoir with a width of 3 mm at the top of the capillary channels. At low-power operation, the excess liquid will gather inside this reservoir, while a continuous liquid flow is ensured at maximum power. The grooves also help to guide the liquid flow smoothly from the reservoir to the evaporator on the straight section. To reduce the entrainment limit, the groove was covered with a mesh layer to reduce the sheer stress and stop the flow in the reservoir, as shown in Figure 4.

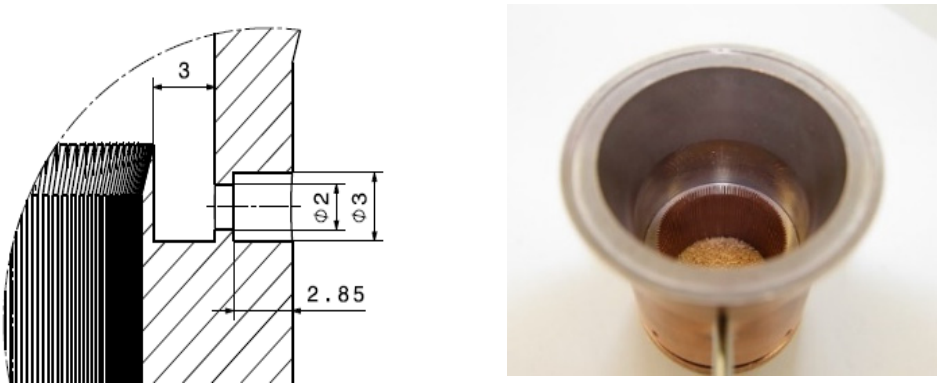

(**a**) (**b**)

Figure 4. Inner view of HPEE mock-up: (**a**) illustration of the reservoir; (**b**) manufactured grooves and sintered porous evaporator.

Besides the reservoir developed as a precautionary measure against flooding, the liquid inventory inside was separated into three steps corresponding to three heat load ranges. The first-round test was conducted with a water volume suitable for a heat load reaching a maximum of 1 MW/m^2, the second round was designed for a heat load ranging from 1 to 5 MW/m^2, and the last round was designed for a 5–20 MW/m^2 heat load. The heat load ranges and their liquid inventories are listed in Table 2.

Table 2. The heat load ranges with their corresponding liquid inventories.

Heat Load Range	Liquid Inventory
0–1 MW/m^2	1.5 mL
1–5 MW/m^2	2 mL
5–20 MW/m^2	2.5 mL

2.4. Condenser

The design of the condenser was mainly governed by considerations related to the calorimetric evaluation of the power transferred by the HPEE. It was performed by measuring the external coolant flow rate, pressure, and temperatures before and after coming into contact with the HPEE condenser's surface, which is discussed in detail in Section 2.6.3. Increasing the temperature difference between the two measurements will reduce the power evaluation uncertainty. As such, a high heat transfer coefficient would allow us to maintain the temperature of the condenser wall at the desired level while using low coolant flow rates, resulting in more considerable temperature differences between the two measurements.

Another critical constraint of the condenser design stems from the vacuum chamber's geometry in which the mock-up is installed. The size of the coolant tube is limited to tube DN65, which has an external diameter of 76.1 mm. Considering the required pipe wall thickness and other mechanical constraints, the condenser's size is limited to a circular area with a diameter of 60 mm.

The condenser's thickness was set to 10 mm according to an examination of the temperature chain along the heat pipe and accounting for the effective heat resistance of various parts [6]. This value was obtained by considering the maximum loading case, i.e., a transferred power of 5.7 kW, and imposing an operating vapor temperature of 200 °C, i.e., the same level as that set for DIV-HP operation.

Since liquid droplets accumulate inside the condenser's surface, a slight slope was added, thereby rendering the condenser wall 2 mm thicker at the margin. With this shape, the calculations show that for the HPEE under maximum loading conditions, the vapor temperature is T_{vapor} = 196.6 °C.

The mock-up has a conical section ranging from 60 mm in diameter at the condenser to 25 mm at the evaporator, as shown in Figure 5. The condenser and the conical part have no grooves so that the manufacturing process was simple and cost-effective. The parameters of the HPEE mock-up are summarized in Table 3.

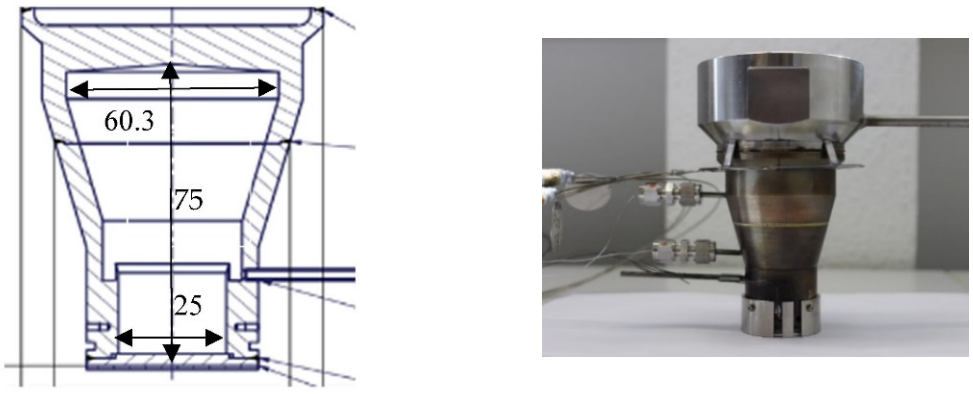

(**a**) (**b**)

Figure 5. HPEE mock-up: (**a**) cross-section through the mock-up with dimensions; (**b**) photograph of the HPEE mock-up.

Table 3. Parameters of HPEE body.

Parameters	Symbol	Value
The outer diameter of the evaporator	$d_{e,o}$	33.4 mm
The inner diameter of the evaporator	$d_{e,i}$	25 mm
The thickness of the evaporator wall (CuCrZr)	t_t	2 mm
Outer diameter of condenser	d_{cond}	60.3 mm
Inner diameter of condenser	d_b	52 mm
The thickness of the condenser wall (CuCrZr)	t_c	10 mm
The inner height of the adiabatic zone	h_{ad}	75 mm
Incision angle	β	19.5°
Evaporator protect plate (W)	t_w	2 mm

2.5. Instrumentation of the HPEE Mock-Up

The mock-up's size and, in particular, the reduced vapor volume dimensions allow for only a limited number of measurements to monitor the heat pipe's operation. Thus, three thermocouples (T-HP05, -HP06, and -HP07) were inserted at different positions in the condenser wall, as seen in Figure 6a. All these sensors were placed at a depth of 5 mm from the condenser's surface. Two thermocouples (T-HP03 and -HP04) monitored the axial change in vapor temperature at two locations: one just above the grooved area and one close to the condenser, as shown in Figure 6b. Four additional thermocouples (T-HP08, -HP09, -HP10, and -HP11) measured the wall temperature near the evaporator: one at the center of the evaporator, the other three being distributed 5.7 and 10 mm away from the center, as indicated in Figure 6c. These sensors were brazed on the surface of the CuCrZr wall directly under the tungsten armor. All thermocouples are K-type with a nominal uncertainty of ±1.5 °C or ±0.4%.

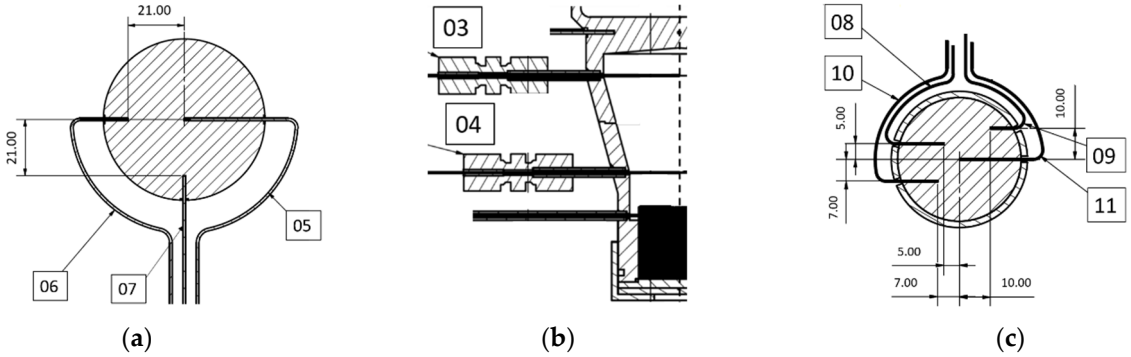

Figure 6. Temperature measurement arrangement of the FHP mock-up: (**a**) condenser wall temperature measurements (T-HP05:HP07); (**b**) vapor temperature measurements (T-HP03:HP04); (**c**) loaded surface temperature measurements (T-HP08:HP11).

2.6. Experimental Setup

The experiment was performed under vacuum conditions to limit the thermal losses due to heat convection (in the air) and protect the heated surface from unwanted oxidation. The mock-up was installed in an existing vacuum tank with a diameter of 50 cm and a height of 100 cm, as shown in Figure 7. This tank was evacuated by a vacuum pump PFEIFFER DUO 35 M, for which the minimum vacuum level that was obtained was 1.6×10^{-2} mBar.

Figure 7. Experimental setup in the laboratory.

2.6.1. Heat Source Systems

In order to apply the load on the surface of the mock-up, the initial plan considered a Diode laser machine, namely, LDF-20000-200 from Laserline. This device can provide power from 0.3 up to 20 kW. However, the zoom laser optic selected for this experiment, OTZ-2, limits the input power to 10 kW. This optic was selected since it can adjust the beam spot from 19 × 19 mm^2 up to 82 × 82 mm^2, thus making it suitable for our experimental purposes. As can be seen in Figure 8c, the beam spot has a rectangular shape with a relatively uniform density in the center.

(**a**)

(**b**)

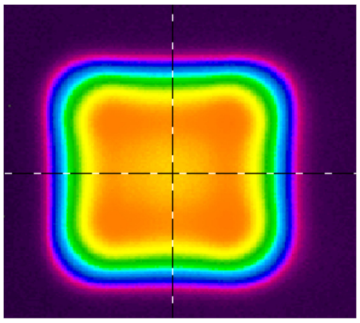

(**c**)

Figure 8. Laserline LDF 20000-200: (**a**) laser machine; (**b**) Zoom laser optic below the vacuum vessel; (**c**) laser spot size 19 × 19 mm^2.

For the purposes of the present experiment, the beam spot was set to its lowest value, 19 × 19 mm^2. With this spot size, assuming a uniform heat deposition, the power of the laser must be incremented from 289 W (1 MW/m^2 averaged surface heat flux) up to 5780 W (20 MW/m^2). As the laser optic cannot be used in the vacuum system, the optics are installed outside the vacuum chamber, with the laser beam passing through a unique vacuum window with a transport efficiency of around 80%.

An electric heater was developed as an alternative or backup solution to the laser machine, which uses a shaped copper block with six heaters and is intended to cover the testing matrix's low power range. Its power is provided by three power supplies via DELTA ELEKTRONIKA SM300-10D.

The block has a diameter of 80 mm and a height of 100 mm on the larger side (where the heaters are inserted), and it reduces its size to only 25 mm towards the heater end that comes into contact with the mock-up. Each heater has a diameter of 12.5 mm, is 80 mm in length, and can provide a maximum power of 800 W (4800 W in total) and operate up to 750 °C.

The copper heater was installed directly under the heat pipe and was placed in direct contact with the evaporator's surface, as in Figure 9. The support structure was isolated

with ceramic parts from the electrical heaters and the copper body to reduce heat loss and avoid current leaks, as in Figure 9b. Four thermocouples monitored the temperature along the copper block axis.

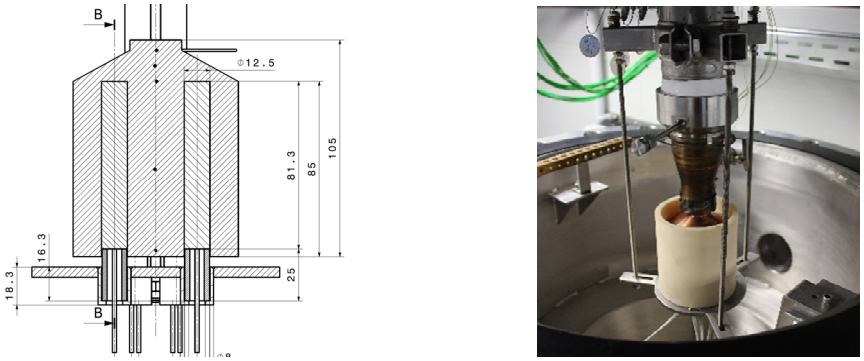

(**a**) (**b**)

Figure 9. Structure of electric copper heater: (**a**) assembly illustration; (**b**) installation with ceramic isolation.

2.6.2. External Cooling System/Heat Sink System for HPEE

We used an external water-cooling circuit to transport the power applied to the HPEE mock-up. As mentioned earlier, the objective is to attain a high heat transfer coefficient outside the condenser region to reduce the uncertainty in the calorimetric evaluation of the transported power. This was achieved by implementing a jet impingement cooling system featuring seven nozzles [9], as shown in Figure 10. An extensive list of the cooling system's parameters is listed in Table 4.

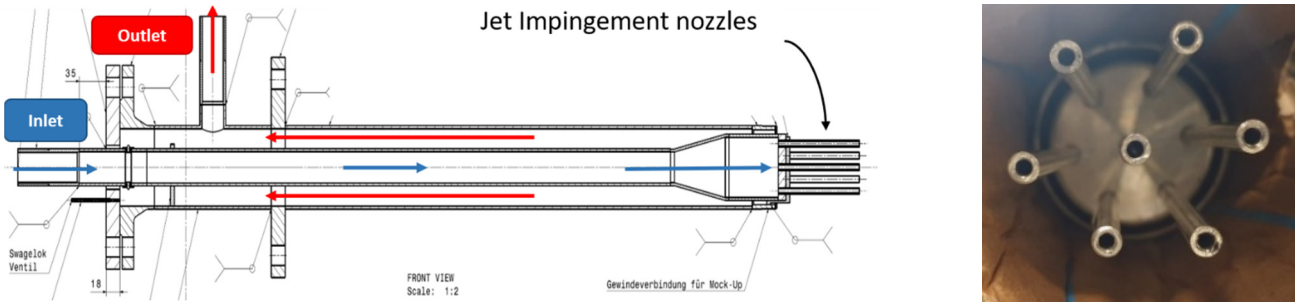

(**a**) (**b**)

Figure 10. Coolant system used for mock-up: (**a**) illustration; (**b**) finalized nozzle heads.

Table 4. Parameters of heat sink system with impinging jet.

Parameters	Symbol	Value
The inlet temperature of the coolant	θ_{in}	20 °C
Pressure	p	4 Bar
The inner diameter of the coolant pipe	$d_{coolant}$	60.3 mm
The thickness of the coolant box wall (steel)	t_{cool}	4 mm
Number of jets	N_n	7
The inner diameter of the jet	D	3 mm
Distance between jet and bottom of FHP	H	15 mm

2.6.3. Calorimetric Evaluation of the Power Applied to the Mock-Up

With the existing experimental setup, estimating transported power by accounting for all heat losses and the surface heat load from the input power readings, either from the laser machine or the electrical heater, is challenging. As an alternative, we used the

calorimetric method to evaluate the power transferred into the coolant system, which is the power transferred by the mock-up. Thus, the calorimetric power is estimated as follows:

$$\dot{Q} = (h(T_{outlet}, p_{outlet}) - h(T_{inlet}, p_{inlet})) * \rho(T_{outlet}, p_{outlet}) * \dot{V}_{outlet} \quad (1)$$

where h is the specific enthalpy (J/kg), and ρ is the density (kg/m^3). Both quantities are calculated based on the provisions of the IAPWS Industrial Formulation 1997 for region 2 [10] using the measured water temperature and pressure. The measurements were made in the vicinity of the inlet/outlet nozzles of the cooling assembly shown in Figure 10 using pressure sensors (OPTIBAR-PM-5060-C, with a measuring range from 0–25 bar, from KROHNE Messtechnik GmbH (Duisburg, Germany)) and resistance thermometers (RTD). To estimate the mass flow, the volumetric flow rate $\dot{V}$ was measured by the water flow meter (HP-F-01 KRONE 250 M40) installed at the heat sink outlet. A complete list of the sensors, their types, and their accuracies are given in Table 5.

Table 5. Parameters of HPEE experiment's measuring instruments applied to heat sink.

Component	Location	Model	Accuracy
Temperature T-01	Coolant inlet	RTD	$\pm(0.15 + 0.002 \times \lvert T \rvert)$ (Class A)
Temperature T-02	Coolant outlet	RTD	[DIN43760]
Pressure P-01	Coolant inlet	PM-5060-C	$\leq \pm 0.5\%$ of span [IEC 61298-2]
Pressure P-02	Coolant outlet	PM-5060-C	
The volume flow rate sensor F-01	Coolant outlet	H250 M40	1.6% of measured value VDI/VDE 3513-2

3. Results

3.1. Consideration of the Evaluation of the Transported Power via the Calorimetric Method

Figure 11a illustrates the evolution of the temperatures recorded at the inlet and outlet of the cooling assembly for a typical loading, which influences the enthalpy estimation, as shown in Figure 11b. In this figure, the loading on the test object is zero until 120 min; then, it is turned on with 300 W, and the outlet temperature increases as expected. It is interesting to remark that even when no net power is applied to the mock-up, the outlet temperature is slightly higher than the inlet value. This behavior is mainly due to the frictional losses of the jet cooling and will need to be accounted for when evaluating the transported power. A bias sensor setup was excluded because the sensors deliver practically the same values without flow.

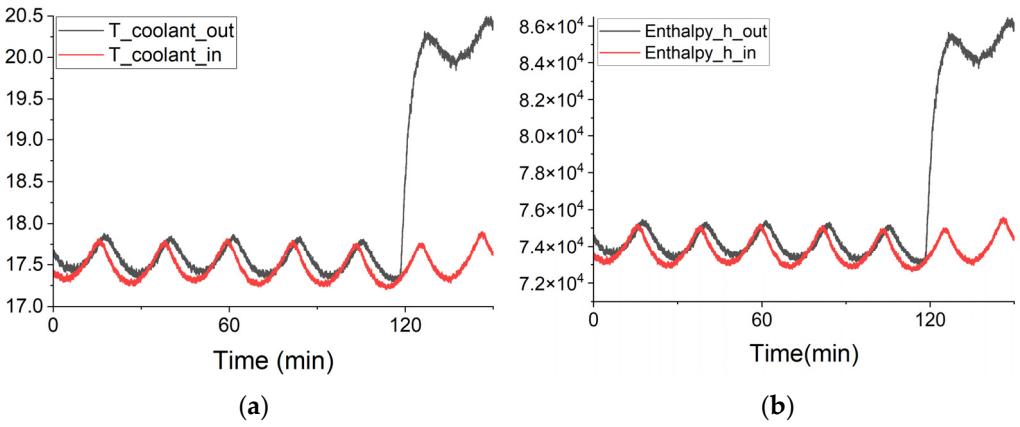

Figure 11. Transient measurement at the coolant inlet and outlet with laser power of 300 W: (**a**) temperature; (**b**) enthalpy.

Another notable finding is the fact that there is a time lag between the two signals. This can be combined with the fact that there is an over-imposed oscillation of the temperature

signals coming from the experimental hall cooling circuit. Therefore, this can lead to an erroneous evaluation of the power if not adequately addressed.

The way to address the latter problem is to first evaluate the time lag *dt* between the outlet temperature measurement and the inlet temperature signal. This dt is calculated for each flow rate setting, and the calculation is repeated at least once a day for a fixed set of parameters by applying the 'finddelay' function in MATLAB. For instance, for a flow rate of 100 L/h, the lag dt is around 1.6 min. Then, a calorimetric power evaluation is carried out using the following formula:

$$\dot{Q} = \left(h\left(T_{outlet}(t), p_{outlet)}(t)\right) - h(T_{inlet}(t-dt), p_{inlet}(t-dt))\right) * \rho(T_{outlet}(t), p_{outlet}(t)) * \dot{V}(t) \quad (2)$$

An example of the data processed in this way is presented in Figure 12 and the original data. By subtracting the time shift, the peak of the inlet enthalpy moved to the same time point as the outlet, and the calorimetric power fluctuation was obviously reduced.

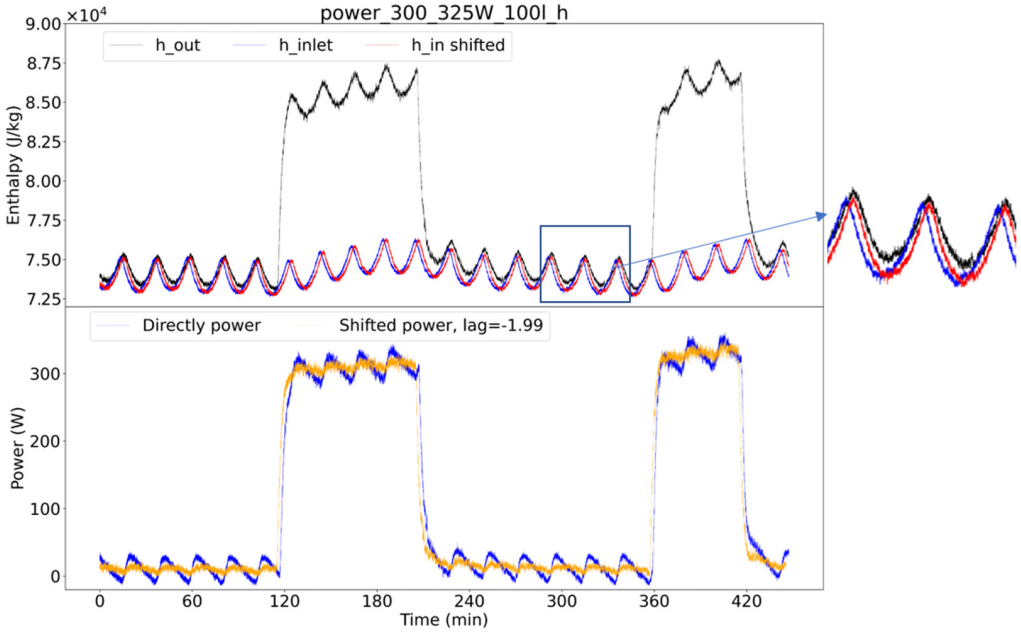

Figure 12. Comparison of the enthalpy and calorimetric evaluation of the power with 300 and 325 W: enthalpy-the red curves indicate the enthalpy calculated at the time earlier than time t with time lag dt; power-the orange curves indicate the power calculated with Equation (2); for comparison, the blue curves show the power calculated without accounting for the time delay.

The average power with and without applying the time shift correction in Figure 12 was compared in a steady state. From this picture, both average powers calculated over each interval when the load was applied or during the dwell time are the same independently of whether we apply the time shift. The only difference is the associated standard deviation, which is significantly higher when we use the raw data. Another finding that can be seen from this figure is that there is always a net power rise of around 10.5 (3.8 W), even when no heat load is applied to the mock-up. As mentioned earlier, this net power is associated with frictional losses due to jet impingement cooling. Thus, when estimating the power applied to the mock-up and, implicitly, the wall heat flux, this power must be subtracted from the power evaluated when the load is applied.

$$P_{applied} = P_{evaluated} - P_{friction} \quad (3)$$

3.2. Temperature Measurements of Mock-Up-1 through the Laser Machine Test

The mock-up was heated with the laser as the heat source in the first series of tests. The amount of water inside the mock-up was 1.5 mL for a maximum of 1 MW/m^2. The evaluated power level started from a low 20 W, at which point the heat flux is around 0.4 MW/m^2 (for safety reasons), and then it was increased stepwise by 0.05 MW/m^2 after each 30 min to obtain a stable value.

The transport power efficiency corresponds to $e = P_{applied}/P_{input}$. The efficiency of laser power below 150 W is between 13% and 47%. Above this level, it stabilizes at around 50%. The reason for this low efficiency became clear at the end of the testing campaign by examining the mock-up surface and the shielding plate placed in front of the mock-up to protect the thermocouple wires from the laser beam. Despite the checks performed during the assembly, the shield plate changed its position and covered almost half of the target, as seen in Figure 13. This led to the improper loading of the mock-up, as the beam hit the steel ring placed around the tungsten armor instead of heating the central part.

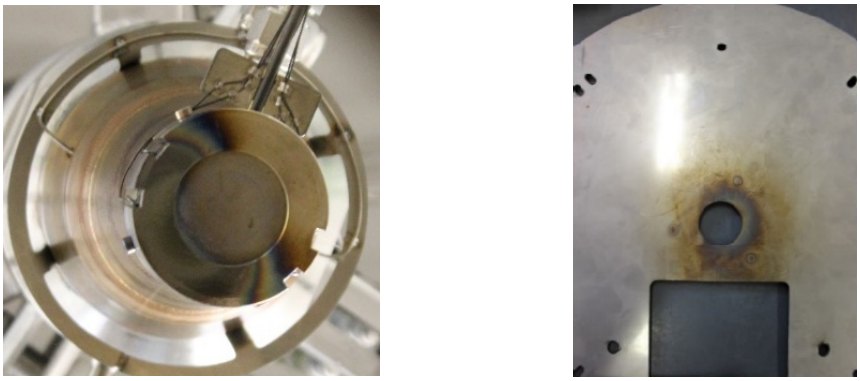

(**a**) (**b**)

Figure 13. Status of the laser-heated surface after the first series of tests: (**a**) mock-up surface—the dark-gray area indicates that the load was applied eccentrically, only partially heating the tungsten armor as intended, wherein a significant part of the load is applied to the steel ring holding the armor; (**b**) shielding plate's surface is heated on the other part.

Meanwhile, the low efficiency meant that the beam power had to be ramped up relatively quickly with modest gains in terms of the transported power. At power levels around 1 kW, the window for allowing the laser to pass through had already reached temperatures so high that the gaskets were damaged. This affected the vacuum in the test chamber. Once this occurred, the testing campaign was interrupted, and the vacuum chamber windows were changed.

Despite the improper loading conditions of the mock-up, the results still provide some helpful information. Figure 14 shows the evolution of the temperatures measured by the thermocouples installed on the mock-up during the three loading cases. In these pictures, one can see that the evaporator temperatures tend to change their values significantly during a (long) testing session. Generally, for a low calorimetric power level of 150 W, the evaporator temperatures stabilize at an initial level, but these temperatures drop to a lower level after a while. For powers of 400 W and 500 W, such a behavior is detected as well, but in a shorter amount of time. This behavior could be related to the vaporization characteristics of the liquid inside.

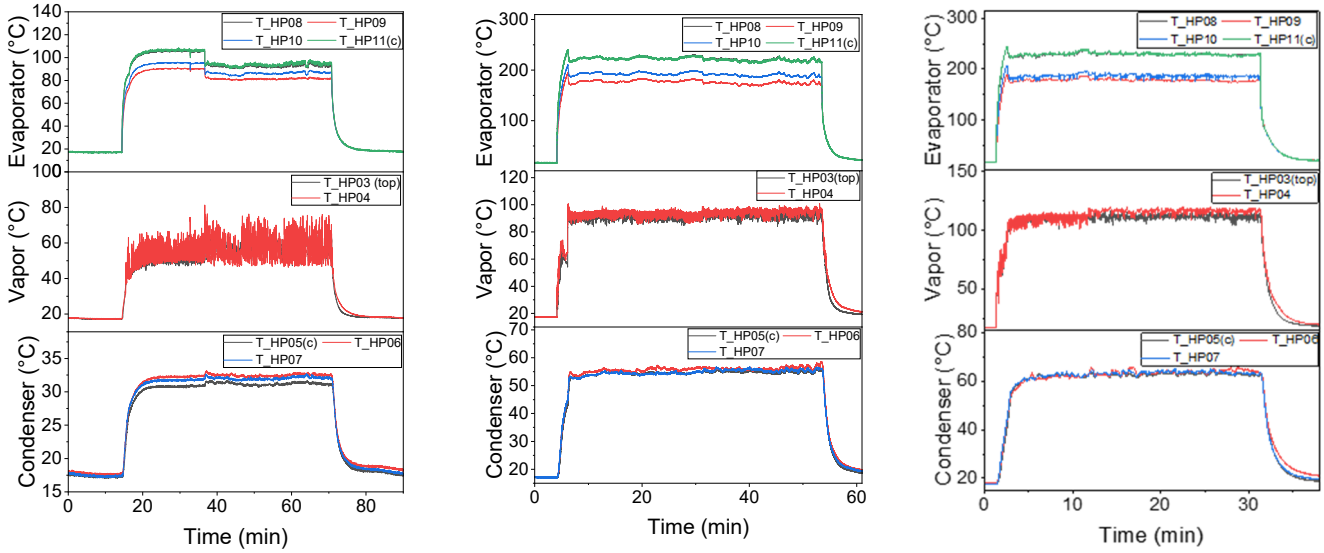

Figure 14. Mock-up-1 temperature evolution with liquid inventory for 1 MW/m^2 and laser calorimetric power: (**a**) 150 W (heat flux: 0.3 MW/m^2); (**b**) 400 W (heat flux: 0.82 MW/m^2); (**c**) 500 W (heat flux: 1.0 MW/m^2).

Liquid vaporization may occur at the liquid–gas interface in cavities containing entrapped vapor. Once nucleation is initiated, the superheat required to sustain bubble formation typically drops to a much lower value. This drop apparently occurs because cavities in the surface are refilled with vapor when nucleation commences. Bubble formation can then be sustained at low superheat levels because vaporization can occur at the liquid–vapor interface within these reactivated cavities [11]. The long duration for the drop of 150 W could indicate that the vapor temperature is not high enough to activate nucleation. Nevertheless, Figure 14b,c clearly show that the evaporator temperature drops simultaneously when the vapor temperature increases. With a higher input power of 500 W, the time required to initiate nucleation is shorter. However, the fact that the heat load was primarily applied on the stainless-steel ring and not on the tungsten armor might also explain the evaporator's erratic behavior.

When plotting the vapor temperature versus the estimated heat flux, Figure 15 shows that the dependence is almost linear. Here, the heat flux was estimated using the calorimetrically estimated power, which is assumed to be applied to the darkened area seen in Figure 13a. This area is estimated to be around 500 mm^2, almost as large as the exposed tungsten surface in front of the evaporator. The vapor temperature at the different positions, HP03 and HP04, shows almost the same value, which means the liquid inside is in a saturated state.

By examining the dependency between the applied heat flux and the superheat ΔT, which is calculated by determining the difference between the average value of the four temperatures near the evaporator and the vapor temperature of the sensor T-HP04 close to the evaporator's surface in Figure 16, we can see that the curve varies linearly up to 200 kW/m^2 but with high uncertainty. The curve shifts towards the left for a higher heat load, and the measurement points seem to spread wider after several repeat tests. This is probably due to the erratic behavior of the heat pipe caused by the abnormal loading conditions. Even so, at up to 1.1 MW/m^2, the curve shows no indication of drying out or partial film boiling on the evaporator's surface. The uncertainty of the applied heat flux is around 23% for a coolant temperature difference of 3.5 °C, whereas it is 87% for 1.0 °C.

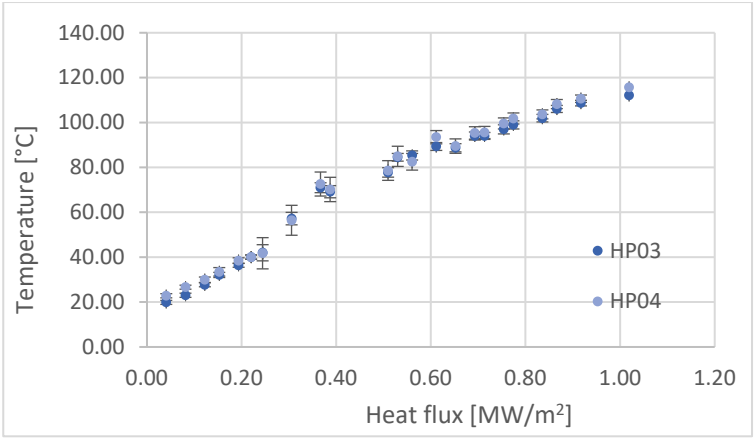

Figure 15. Vapor temperature of mock-up-1(heated by laser power) as a function of the heat flux.

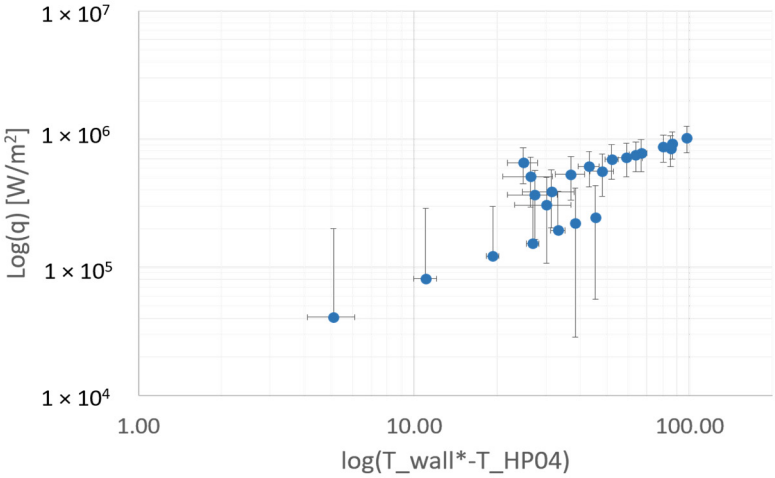

Figure 16. Heat flux versus average wall superheated ΔT of mock-up 1 with laser.

These results indicate that the poor loading conditions of the first experimental setup hamper the interpretation of the results. Consequently, to better understand the heat pipe behavior at the lower range of loading conditions, it was decided to switch from laser heating to a more conventional form, namely, the use of a shaped electric copper heating element.

3.3. Temperature Measurements of Mock-Up-1 via the Electric Copper Heater Test

To more effectively control the applied power, it was decided to temporarily use a different heating method, namely, an electrical heater, until the issues encountered during laser heating were solved. The power was increased in the same manner as with the laser. Compared with the rapid heat loading of the laser applied to the evaporator, the ramp-up is slower in the case of the electrical heater. It takes about two hours for a particular power setting to achieve a stable temperature trend both on the mock-up and the copper block. Since we intended to compare the results of the two distinct heating methods, the filling and the cooling conditions were maintained as before.

From the data recorded, one can see in Figure 17 that the present setup offers better heating conditions than before. The ratio between the electric input power and the one estimated calorimetrically is around 85%.

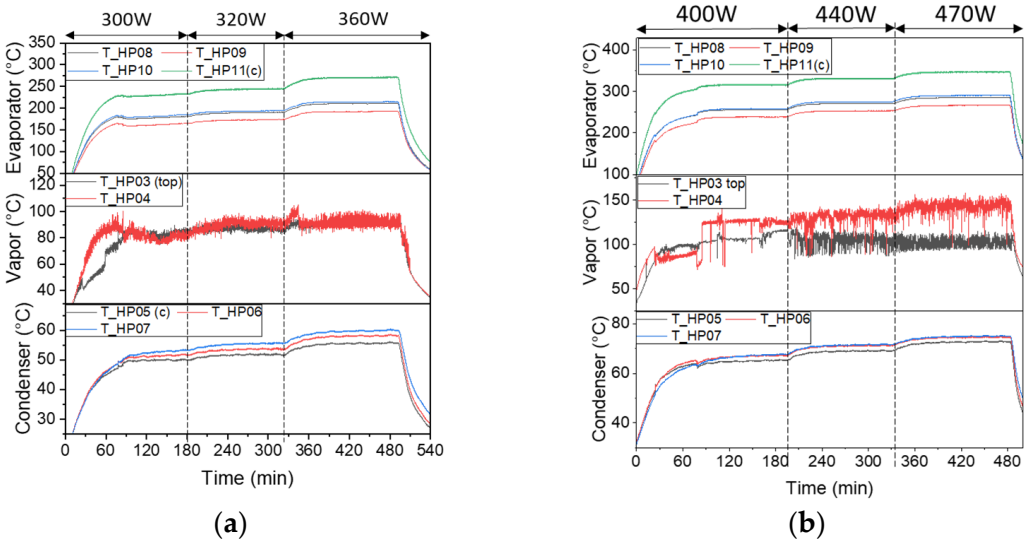

Figure 17. Mock-up-1 temperature evolution with liquid inventory for 1 MW/m^2 and electric copper heater calorimetric power: (**a**) 300, 320, and 360 W (heat flux: 0.61, 0.65, and 0.73 MW/m^2); (**b**) 400, 440, and 470 W (heat flux: 0.82, 0.9, and 0.9 MW/m^2).

Comparing the temperatures at the three positions (those of the evaporator, vapor, and condenser) of the mock-up, the evaporator temperatures have a much smoother evolution than the ones obtained with the laser. During the testing with electric power, it was observed that the two vapor temperatures started to separate at high heat loads of around 0.9 MW/m^2. When comparing the vapor temperature plots from Figure 17a,b, the two temperatures are practically identical for low powers (Figure 17a). However, for the high loadings (Figure 17b), the measurement of T-HP04 close to the evaporator increases by 40 °C while the one of T-HP03 close to the condenser stays around 100 °C even when the loading is increased.

For the laser test, despite the erratic behavior and faulty loading, a heat pipe effect could be observed, as the evaporator temperatures dropped sharply after an initial rise, and the vapor temperature at the two positions remained the same as those in Figure 14. By examining the electric copper heater temperature trends, it can be observed that there is little evidence of mock-up-1 acting as a heat pipe after the two vapor temperatures separate.

When plotting the temperature difference between the evaporator and condenser as a function of the transferred power, the results of mock-up-1 with an electric copper heater follow the same trend as for the case when there is no liquid evaporation inside the heat pipe. It means that the heat transfer occurs only through conduction (solid line in Figure 18). For the tests performed with the laser, this parameter follows the heat conduction trend up to around 200 W, and then diverges from it and shows a tendency of saturation at lower values as would be expected from a heat pipe. This observation led us to conclude that mock-up-1 might not have been tight and might have been losing water so that it no longer operated as a heat pipe. Then, a leakage at the connection between the water feed pipe and the valve was found after removing the mock-up from the test rig. The mock-up itself showed no signs of damage despite the early eccentric loading of the heat pipe head.

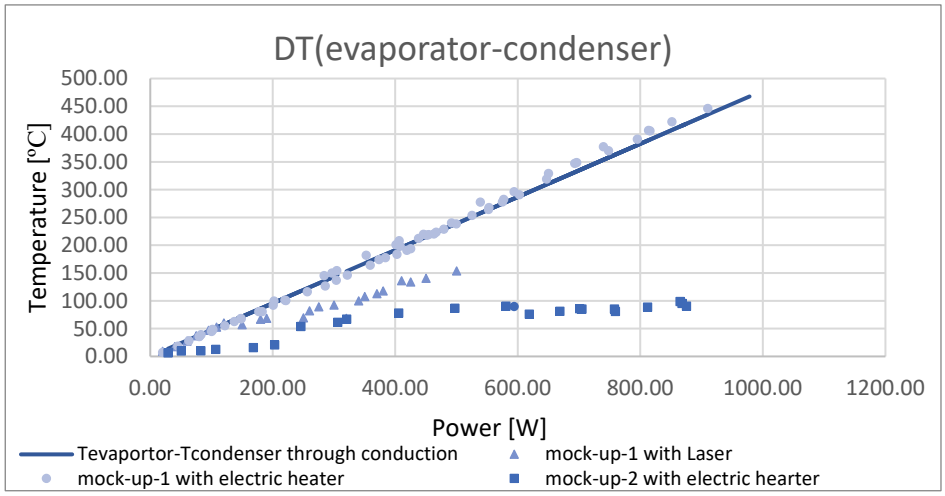

Figure 18. Variation in the temperature drop between the evaporator and condenser with the transferred power for all testing campaigns.

3.4. Temperature Measurements of Mock-Up-2 via the Electric Copper Heater Test

As the first mock-up needed to be repaired, mock-up-2, featuring an improved evaporator, was installed and tested. Figure 19 shows the temperature evolution for this new mock-up. In comparison, the sharp drop in the temperature due to the onset of boiling is not easily detectable as in the laser test because of the slower ramp up. Comparing these curves with those in Figure 17 shows that mock-up-2 stays much colder than the previous case. The evaporator and vapor temperature remain relatively constant in the axial direction after heat flux reaches 0.6 MW/m^2. At low heat fluxes, the evaporator temperatures stabilize rather quickly, and the four temperatures have similar values. Starting from 0.6 MW/m^2, after an initial evolution similar to the lower loadings, the evaporator temperatures suddenly jump to 100 °C, and the recoded values show significant spreading. This behavior indicates a change in the operating regime of the heat pipe that resulted in an increase in the wall temperature.

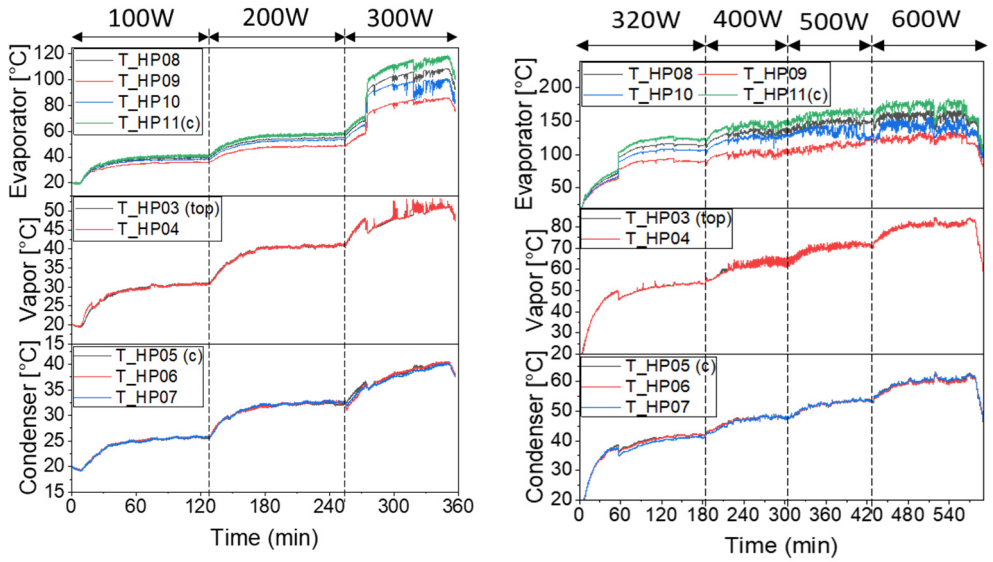

(**a**) (**b**)

Figure 19. Mock-up-2's temperature evolution with liquid inventory for 1 MW/m^2 and electric copper heater calorimetric power: (**a**) 100, 200, and 300 W (heat flux: 0.2, 0.4, and 0.6 MW/m^2); (**b**) 320, 400, 500, and 600 W (heat flux: 0.65, 0.8, 1.0, and 1.2 MW/m^2.

In Figure 18, it can be gleaned that the mock-up more clearly operates as a heat pipe, and the variation in the temperature difference between the evaporator and condenser versus power is plotted. In the case of mock-up-2, the measured values quickly diverge from the heat conduction trend and saturate at around 100 °C for power levels above 400 W.

A saturation trend similar to that shown for mock-up-1 with laser heating can be observed by analyzing the vapor temperature dependence on the applied heat flux, as shown in Figure 20, where T_HP03 and T_HP04 remain almost the same and increase linearly with heat flux.

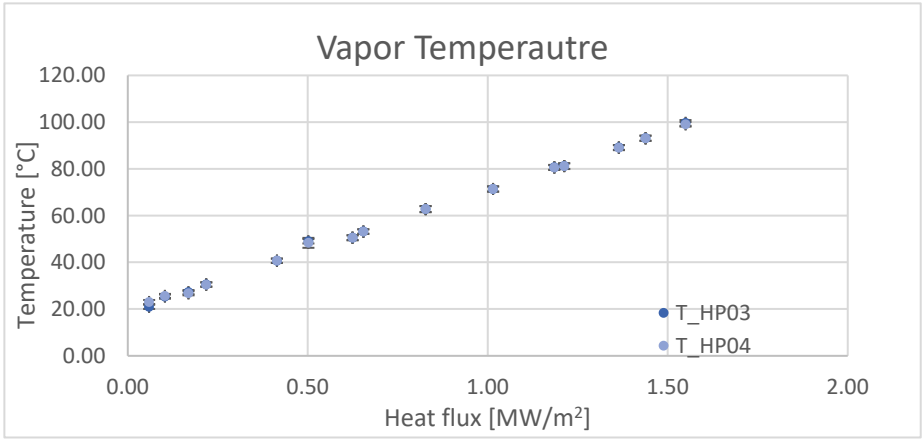

Figure 20. Vapor temperature of mock-up-2 with electric heater as a function of the heat flux.

By observing the superheat dependence on the applied heat flux, as shown in Figure 21, the degree of saturation starts to become more noticeable when the heat fluxes are above 1 MW/m^2, corresponding to a transferred power of about 500 W. The results indicate that this transition is associated with the onset of nucleate boiling. When the heat flux increases, the system state jumps horizontally to the nucleate boiling curve [11].

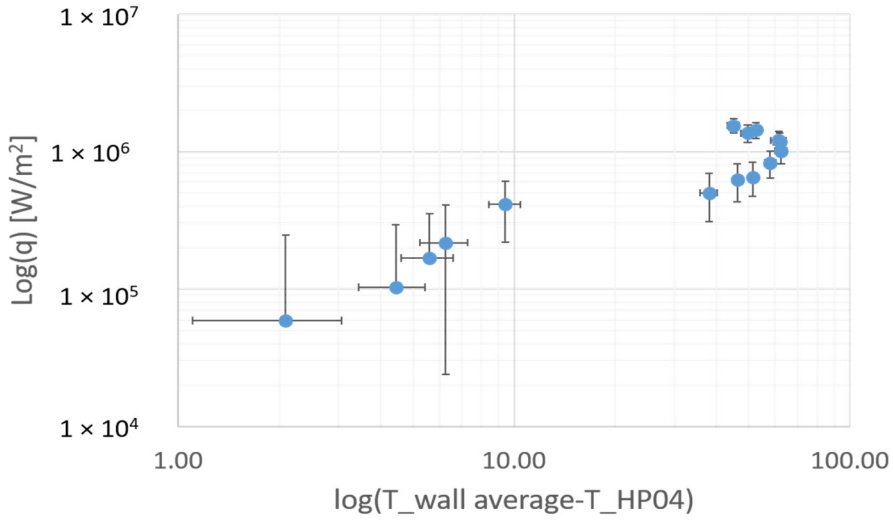

Figure 21. Heat flux versus average wall superheated ΔT of mock-up 1 heated via electric heater.

4. Conclusions

The experimental investigation of a heat pipe evaporator's operating limits with a liquid inventory of 1.5 mL, a heat flux until 1 MW/m^2, and with a laser and an electric copper heater applied as heat sources has produced an initial series of results. These results indicate that both the developed mock-ups can operate well until 1.3 MW/m^2, which means that the HPEE can superiorly function as a heat pipe in the designed heat flux range of 1 MW/m^2. Unfortunately, the loss of tightness of mock-up-1 did not allow for a proper

comparative evaluation of the performances of mock-up-2 with an enhanced evaporator. Nevertheless, the performance of the enhanced evaporator seemed very promising.

The experimental setup was extended during the tests by switching the heating method from a laser beam to an electrical heater for the low range of applied loads. The experiment has shown that both heat sources have some advantages and disadvantages:

- The laser heat source can heat the evaporator immediately without requiring other heat transport material and can operate at a high heat flux level. However, the problem of alignment renders the heated surface difficult to control; further, this method is limited by the maximum laser window working temperature of 150 °C at 1 kW laser power. Above this temperature, the vacuum tightness is compromised due to the loss of the gasket's elasticity and the signs of the deterioration of the window material, for which the latter had to be replaced.
- The electric copper heater can effectively heat the evaporator at the correct position. However, a very long time is required to reach a steady state for full power, and a step-wise application of the heating power to the mock-up is impossible. An electric copper heater's maximum heat flux is around 2 MW/m^2 due to its working temperature of 750 °C.

The results so far indicate the potential of using the enhanced evaporator to handle high heat fluxes in a heat pipe, and the plain evaporator seems to show good performance, at least up to 1 MW/m^2. However, due to various technical issues, the loadings are still only at a low range of interest. Electric heating can continue to cover the lower experimental range (200 kW/m^2 up to 1.5 MW/m^2). Furthermore, the alignment of the laser optic with the evaporator solutions must be monitored so that the mock-up can be tested with a higher heat flux level.

The plan for future research is to focus on completing the testing program for the two mock-ups. Later experiments will continue with mock-up-2, which was already installed on the test rig in the first phase, using an increased water quantity inside the heat pipe for higher heat fluxes during the test. Once mock-up-1 is repaired, it will be tested following the same program as that involving the enhanced evaporator.

Author Contributions: Conceptualization, W.W. and B.-E.G.; methodology, W.W., B.-E.G. and W.H.; Formal analysis, W.W.; Data curation, W.W.; Writing—original draft, W.W.; Writing—review & editing, B.-E.G.; Visualization, W.H., J.S. and R.S.; Supervision, B.-E.G., W.H., J.S. and R.S.; Funding acquisition, B.-E.G. All authors have read and agreed to the published version of the manuscript.

Funding: This work has been carried out within the framework of the EUROfusion Consortium, funded by the European Union via the Euratom Research and Training Programme (Grant Agreement No 101052200-EUROfusion). Views and opinions expressed are however those of the author(s) only and do not necessarily reflect those of the European Union or the European Commission. Neither the European Union nor the European Commission can be held responsible for them.

Data Availability Statement: The data presented in this study are available from the corresponding author on reasonable request.

Conflicts of Interest: The authors declare no conflict of interest.

References

1. You, J.H.; Visca, E.; Barrett, T.; Böswirth, B.; Crescenzi, F.; Domptail, F.; Fursdon, M.; Gallay, F.; Ghidersa, B.E.; Greuner, H.; et al. European Divertor Target Concepts for DEMO: Design Rationales and High Heat Flux Performance. *Nucl. Mater. Energy* **2018**, *16*, 1–11. [CrossRef]
2. Makhankov, A.; Anisimov, A.; Arakelov, A.; Gekov, A.; Jablokov, N.; Yuditskiy, V.; Kirillov, I.; Komarov, V.; Mazul, I.; Ogorodnikov, A.; et al. Liquid Metal Heat Pipes for Fusion Application. *Fusion Eng. Des.* **1998**, *42*, 373–379. [CrossRef]
3. Bolt, H.; Kohlhaas, W.; Duwe, R.; Gervash, A.; Linke, J.; Mazul, I. Heat Flux Experiments on Heat Pipes for Plasma Facing Applications. 1995. In Proceedings of the European Symposium on Fusion Technology (SOFT-18), Karlsruhe, Germany, 22–26 August 1994.
4. Rosenfeld, J.; Lindemuth, J. Evaluation of Porous Media Heat Exchangers for Plasma Facing Components. *Proc.—Symp. Fusion Eng.* **1993**, *2*, 1210–1213. [CrossRef]

5. Wen, W.; Ghidersa, B.E.; Hering, W.; Starflinger, J.; Stieglitz, R. Heat Pipe Technology Based Divertor Plasma Facing Component Concept for European DEMO. *Fusion Eng. Des.* **2021**, *164*. [CrossRef]
6. Stephan, P. N5 Heat Pipes. In *VDI Heat Atlas*, 2nd ed.; Springer: Berlin/Heidelberg, Germany, 2010; pp. 1503–1514.
7. Hwang, G.S.; Fleming, E.; Carne, B.; Sharratt, S.; Nam, Y.; Dussinger, P.; Ju, Y.S.; Kaviany, M. Multi-Artery Heat-Pipe Spreader: Lateral Liquid Supply. *Int. J. Heat Mass Transf.* **2011**, *54*, 2334–2340. [CrossRef]
8. Guichet, V.; Jouhara, H. Condensation, Evaporation and Boiling of Falling Films in Wickless Heat Pipes (Two-Phase Closed Thermosyphons): A Critical Review of Correlations. *Int. J. Thermofluids* **2020**, *1–2*, 100001. [CrossRef]
9. Schabel, W.; Martin, H. G10 Impinging Jet Flow Heat Transfer. In *VDI Heat Atlas*, 2nd ed.; Springer: Berlin/Heidelberg, Germany, 2010; pp. 745–751.
10. Kretzschmar, H.-J.; Wagner, W. *International Steam Tables*, 3rd ed.; Springer: Berlin, Germany, 2019. [CrossRef]
11. Carey, V.P. Chapter 7 Pool Boiling. In *Liquid-Vapor Phase-Change Phenomena*; CRC Press Taylor&Francis Group: New York, NY, USA, 2020; pp. 249–330.